Aspects of Orientation-Dependent Grain Growth in Extra-Low Carbon and Interstitial-Free Steels during Continuous Annealing

J.L. BOCOS, E. NOVILLO, M.M. PETITE, A. IZA-MENDIA, and I. GUTIERREZ

The present work concentrates on the application of orientation imaging microscopy (OIM) based on the electron backscattered diffraction (EBSD) technique to the investigation of the microstructural evolution of an extra-low carbon (ELC) steel and a Ti-Nb–bearing interstitial-free (IF) steel, during continuous annealing. Aspects like the nucleation, the evolution of the recrystallized volume fraction and grain size of grains with different orientations, the interface area limiting recrystallized {111} regions, and the apparent growth rates have been considered. Different criteria have been applied in order to identify crystallites produced during annealing. During the first stages of annealing, a network of grain boundaries with misorientations higher than 10 deg is produced, mainly inside the deformed γ-fiber grains. The crystallites formed within this network, free from cells or subgrains at their interiors, can be considered as potential nuclei. However, among all, only some of them become effective due to an important selection. The {111} recrystallized grains have a significant size and number advantage as compared with other texture components, and a hard impingement between clusters of {111} grains is produced during grain growth. The effect of grain growth behind the recrystallization front seems to be negligible as compared with the grain coarsening produced by the migration of this front, driven by the cold-work stored energy.

I. INTRODUCTION

AN important amount of research work has focused on the investigation of recrystallization and texture evolution during annealing of cold-rolled low-carbon steel sheets, and some excellent reviews have been written on the subject.[1–4] A strong γ-fiber texture ({111} plane parallel to the rolling plane) is mainly responsible for the high formability of interstitial-free (IF) and low-carbon steels. Historically, two main theories, based on oriented nucleation[5,6,7] and selective growth,[8,9] competed for the explanation of the texture development during recrystallization. Some attempts have also been made to find complementary approaches based on a frequency advantage or size advantage.[10,11]

During recent years, orientation imaging microscopy (OIM) techniques have been successfully applied, in addition to the more conventional X-ray diffraction and transmission electron microscopy, to investigate the mechanisms behind texture development.[12,13] It is well accepted that the stored energy of cold work distributes heterogeneously according to different texture components,[5] leading to the preferential nucleation on the γ-fiber grains. This has been used as an argument for the development of such texture components. On the base of OIM experimental results, nucleation has been recently described in connection with the deformation microstructure.[14] According to this work, nucleation in deformed {111} IF steel grains seems to be connected with abnormal subgrain growth driven by high misorientations being present inside the grains, some of them being in excess of 10 deg. The presence of such large intragranular misorientations seems to give some advantage to certain subgrains in terms of mobility for abnormal subgrain coarsening. It is suggested[14] that normal subgrain coarsening produces polygonalization, while abnormal subgrain growth leads to nucleation.

The OIM technique has also been used to investigate grain-boundary migration during recrystallization for grains belonging to different texture components in aluminum[15,16] and IF steels.[7] It has also been used to investigate the grain-size and volume evolution of certain texture components and to determine the growth rate of growing grains with particular crystallographic orientations.[10,11,17]

On the other hand, efforts have been made to model the recrystallization kinetics, using different approaches. Nucleation is very often, for example, considered to obey site-saturation conditions,[18] which means that all the grains are present at the beginning of the recrystallization. This overcomes the inherent difficulties encountered when trying to model nuclei formation concurrent with recrystallization and reduces the problem to a question of grain coarsening produced by the recrystallization-front motion, this last being driven by the difference in the stored energy between recrystallized and deformed structures. It is also generally accepted for modeling purposes that normal grain growth only operates after the completion of recrystallization. However, as soon as the recrystallized grains impinge, it could be assumed that normal grain growth also takes place behind the recrystallization front. There is an increasing tendency to develop models integrating recrystallization and grain-growth kinetics and texture evolution. However, before the full development of such models may occur, more experimental work is required to better understand the mechanisms behind such processes.

J.L. BOCOS, formerly Researcher with CEIT, is Researcher, Fundacion CETENASA, C.P. 31110, Noain, Navarra, Spain. E. NOVILLO, Doctoral Student, M.M. PETITE and A. IZA-MENDIA, Researchers, and I. GUTIERREZ, Principal Researcher, are with CEIT and TECNUN (University of Navarra), 20018 Donostia-San Sebastian, Basque Country, Spain. Contact e-mail: igutierrez@ceit.es

Manuscript submitted February 18, 2002.

Table I. Steel Compositions (Weight Percent)

Steel	Pct C	Pct Mn	Pct P	Pct Si	Pct Al	Pct N	Pct Ti	Pct Nb
ELC	0.040	0.200	0.010	0.007	0.030	0.003	—	—
Ti + Nb-IF	0.003	0.120	0.007	0.007	0.041	0.002	0.019	0.025

In the present work, aspects of the evolution of the recrystallization from the first stages have been investigated, with a special emphasis on the nucleation and grain coarsening of different texture components during recrystallization and grain growth. Quantitative metallography has been performed on the OIM maps, and aspects such as the size/number advantage of the main texture components have been considered. The results have also been used to investigate the validity of the site-saturation hypothesis and to estimate the importance of the grain coarsening behind the recrystallization front. The work has been carried out on a nonstabilized extra-low carbon (ELC) steel and a Ti-Nb–bearing IF steel under the nonisothermal condition usually encountered in industrial continuous annealing lines.

II. EXPERIMENTAL

In the present work, two different cold-rolled steel sheets have been used, whose compositions are shown in Table I. The first of them is an ELC steel, and the second is a Ti-Nb IF steel. These steels have been industrially hot rolled in the roughing mill from 215 to 40 mm and, subsequently, hot rolled at the laboratory to 3.6 mm in thickness. The cold rolling has been carried out at the laboratory, leading to a reduction of 90 pct for the ELC steel and of 87 pct for the IF steel.

These steels have been laboratory annealed following interrupted heating cycles. The final temperatures of the interrupted cycles were 600 °C, 620 °C, 640 °C, and 750 °C for the ELC steel and 700 °C, 715 °C, 725 °C, and 750 °C for the IF steel. On reaching these temperatures, the annealing was interrupted, by cooling directly to room temperature at a rate of about 25 °C/s. The same heating rate of 6 °C/s has been applied for all the experiments. Complete annealing cycles, including a soaking stage after the mentioned heating, have also been applied to some samples. A 70-second soaking time was applied at a constant temperature (750 °C) to the ELC steel. In the case of the IF steel, the temperature increased from 750 °C to 810 °C during this stage, at a rate close to 0.9 °C/s. Afterward, the samples were cooled from the soaking temperature to 680 °C in 27 seconds, followed by a subsequent cooling to room temperature at a lower rate.

Texture measurements have been carried out by the use of X-ray diffraction. The "MTM-HFM" program[19] has been used to determine the orientation distribution function (ODF). Orientation imaging has been carried out in a PHIL IPS* XL30cp scanning electron microscope, using the TexSEM Laboratories MSC 2200 equipment. The spatial resolution of the equipment is about 0.2 μm.

*PHILIPS is a trademark of Philips Electronic Instruments Corp., Mahwah, NJ.

For this purpose, the samples were polished on the rolling plane with colloidal silica to reveal the microstructure. Quantitative metallography has been carried out on the electron backscattered diffraction (EBSD) orientation images, for different texture components. The considered components were the γ-fiber grains having the {111} plane perpendicular to the normal direction (ND) and, belonging to this fiber, the F:{111}⟨112⟩ and the E:{111}⟨110⟩ components; as well as the cube grains having the {100} plane perpendicular to the ND. In certain cases, the grains with the {110} plane perpendicular to the ND have also been considered. The orientation tolerance, for the definition of the texture components, has been 15 deg for all the cases. The rest of the grains that cannot be identified within these categories have been called the "others."

Partially and fully recrystallized samples have been analyzed, and the criterion for grain definition in a partially recrystallized microstructure has been defined initially as follows. Recrystallized grains have been identified as those resolvable regions with a high-quality factor and no resolvable cells or subgrains at their interiors and being surrounded by grain boundaries presenting misorientations higher than 10 deg.

The sizes of all the grains fulfilling these conditions have been computed by quantitative metallography methods for the different aforementioned components. The mean grain size has been expressed in terms of the equivalent diameter, and the distribution of sizes has been computed. The interfacial area limiting clusters formed by recrystallized grains with a given orientation of {*hkl*} and either the recrystallized or nonrecrystallized regions surrounding them ($S_v^{\{hkl\}}$) has been determined by counting the intersections, per unit area, with the boundary limiting them. The same type of procedure has also been applied to determine the interfacial area between recrystallized and deformed regions ($S_v^{\{Rex\}}$).

The recrystallized and softened fractions (X_v and X_s, respectively) have been determined by quantitative metallography methods and from HR30T hardness measurements, respectively, according to the following expression:

$$X_s = \frac{H_0 - H_i}{H_0 - H_f} \quad [1]$$

With H_0, H_i, and H_f being the hardness after cold rolling, at each stage during recrystallization, and in the fully recrystallized condition, respectively.

III. RESULTS

The OIM image quality maps in Figures 1 and 2 show the evolution of the microstructure, as a function of the annealing conditions, for the ELC and the IF steels, respectively. For the ELC steel, the recrystallization starts during the heating step. The quenching from 600 °C reveals recrystallization at its first stages. The recrystallized grains are small in size and appear, in many cases, to form small clusters. The sample quenched from 640 °C shows a nearly complete recrystallization. It is clear that this steel fully recrystallizes before the onset of the isothermal holding stage

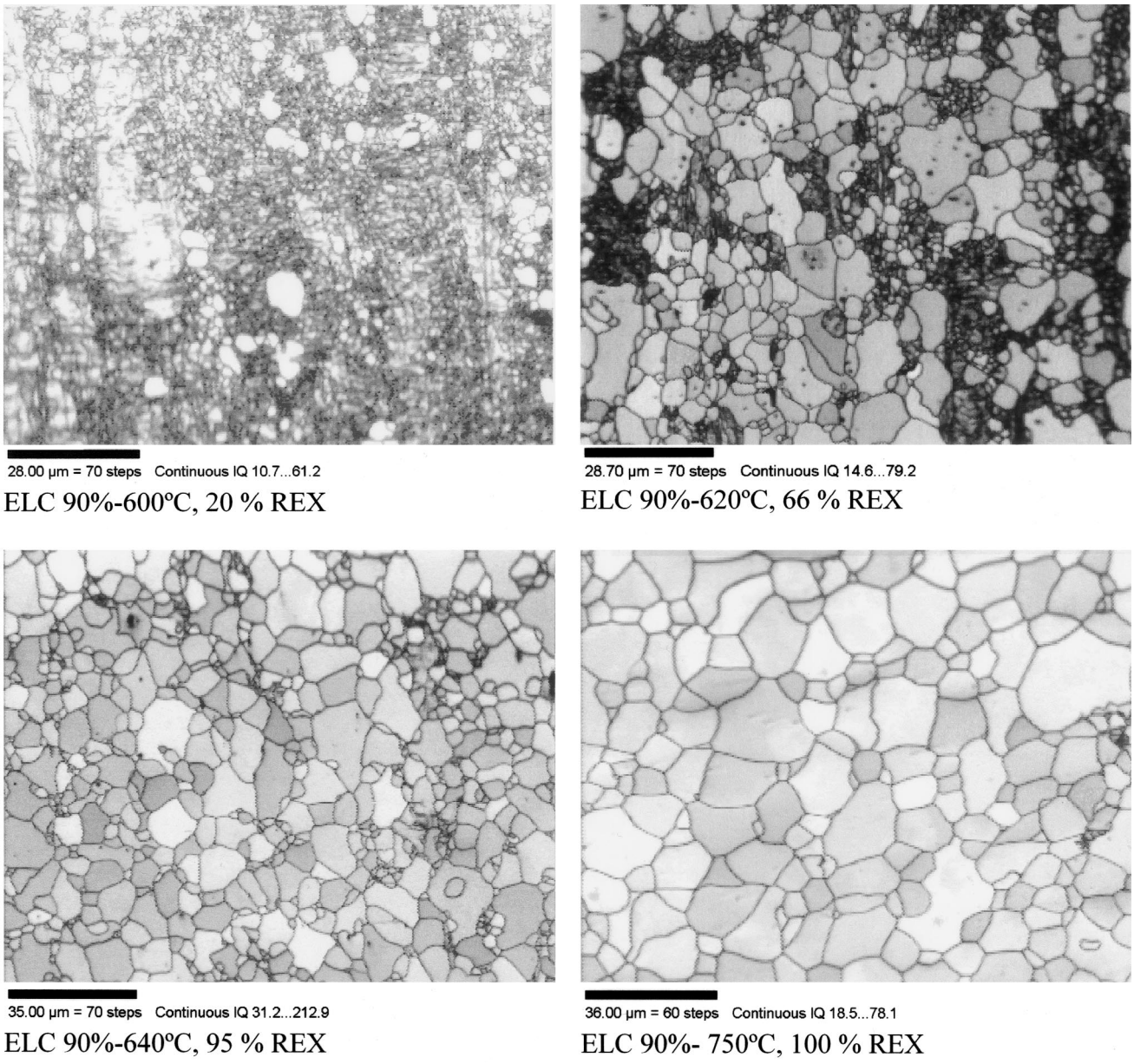

Fig. 1—OIM images showing the microstructure evolution in the ELC steel, as a function of the annealing conditions.

in the complete continuous annealing cycle. The fully annealed sample shows a larger-grain-size microstructure than that before soaking. The main difference arises from the disappearance of the small grains remaining in the microstructure up to the completion of recrystallization.

In the IF steel, the start of the recrystallization also takes place during the heating step, but at a higher temperature (slightly lower than 700 °C) than in the ELC steel. The sample quenched from 700 °C shows a low recrystallized fraction. Fine grains are observed in the microstructure, which are concentrated in certain areas, while at other locations the deformed microstructure seems to remain without any signs of recrystallization. The clustering of the recrystallized grains is more evident in the sample quenched from 715 °C. The recrystallization finishes just before the soaking stage, where it goes from 750 °C to 810 °C at a lower heating rate (~0.9 °C/s). During this last stage, some grain growth of the recrystallized grains is clearly apparent, mainly due, as observed for the ELC steel, to the disappearance of the smallest grains.

The graph in Figure 3 shows the evolution of the recrystallized and softened fractions in both steels, as a function of the temperature of quenching within the annealing cycle. It is to be mentioned that the recrystallized and the softened fractions are very similar, mainly for the case of the ELC steel. For the IF steel, a limited agreement is observed, mainly at low recrystallized fractions. It is clear that the recrystallization kinetics is faster for the ELC steel than for the IF steel. The recrystallization starts in the IF steel when it is close to completion in the ELC steel.

In Figure 4, the evolution of the ODFs obtained from the X-ray measurements is shown, for the cold-rolled, partially, and fully annealed conditions. In the cold-rolled samples and at a low recrystallized fraction, the intensity mainly concentrates along the α-fiber, with levels 14 and 17 times random for the ELC and the IF steels, respectively. Besides, a

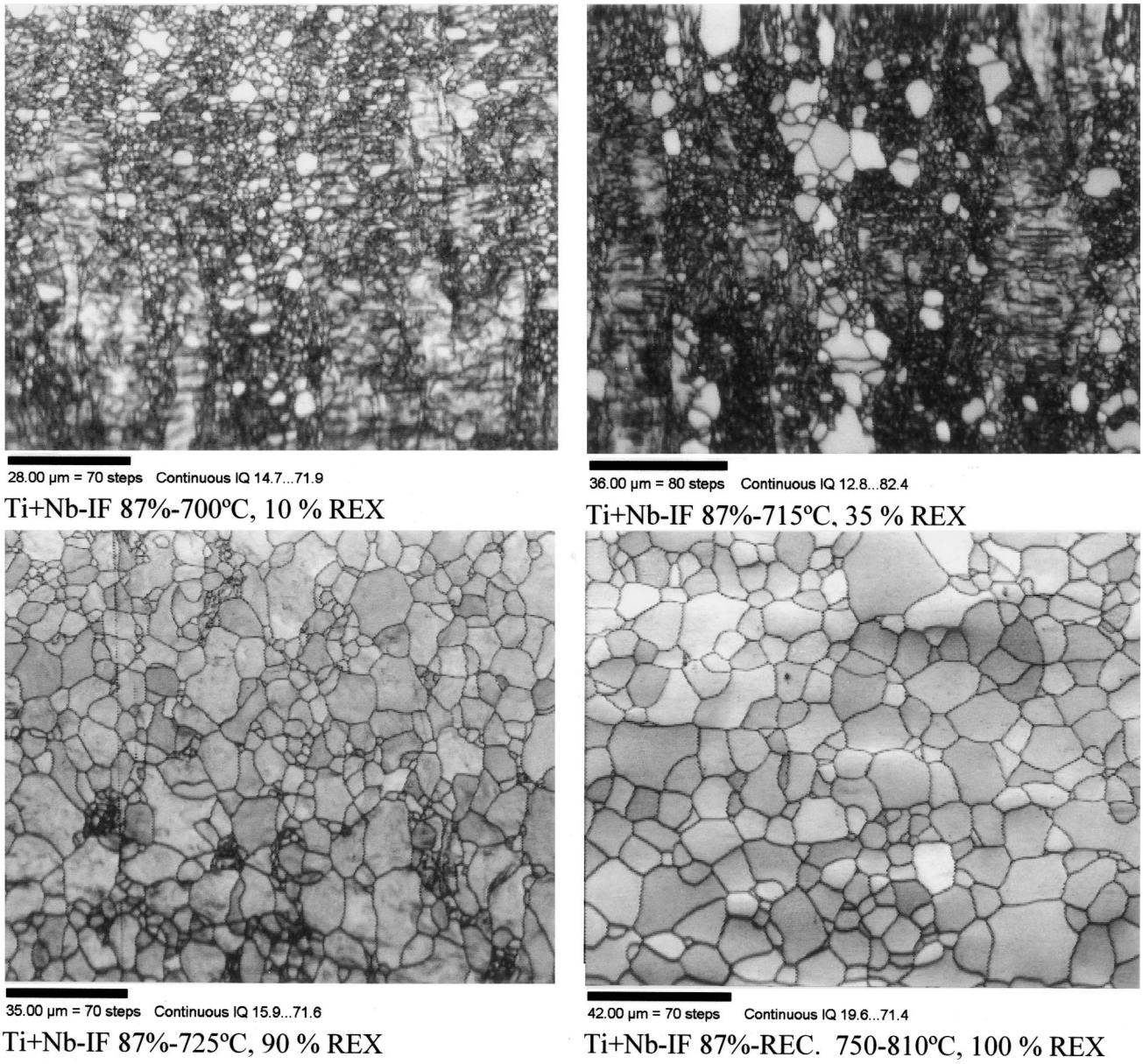

Fig. 2—OIM images showing the microstructure evolution in the Ti-Nb-IF steel, as a function of the annealing conditions.

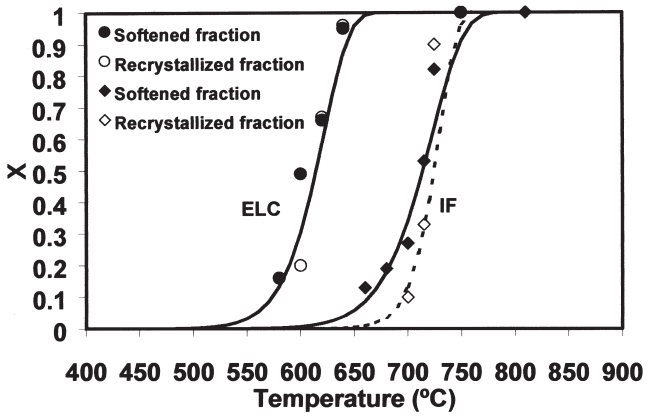

Fig. 3—Evolution of the fraction recrystallized, as a function of the temperature of the quenching.

maximum at the {100}⟨110⟩ cube rotated component, having this same level of intensity, appears. Along the γ-fiber the intensity is 8 and 7 times random, respectively. As recrystallization progresses, the evolution of the texture is relatively small for both steels. The main changes in the ODFs of both steels are observed close to the completion of the recrystallization and afterward. The fully annealed sample has developed an intense γ-fiber with two maxima located close to the {111}⟨112⟩ orientations. The position of the maxima for the ELC and IF steels can be identified as {544}⟨225⟩.

On the OIM images obtained for the different annealing conditions, the recrystallized grains have been divided into different classes, depending on their orientation. The first class includes all the γ-fiber grains showing a {111} orientation within a tolerance of 15 deg. The second class refers to the {100} grains within the same tolerance. Finally, the rest of the grains are those belonging to neither of the two previous classes and are referred to as being "other." The

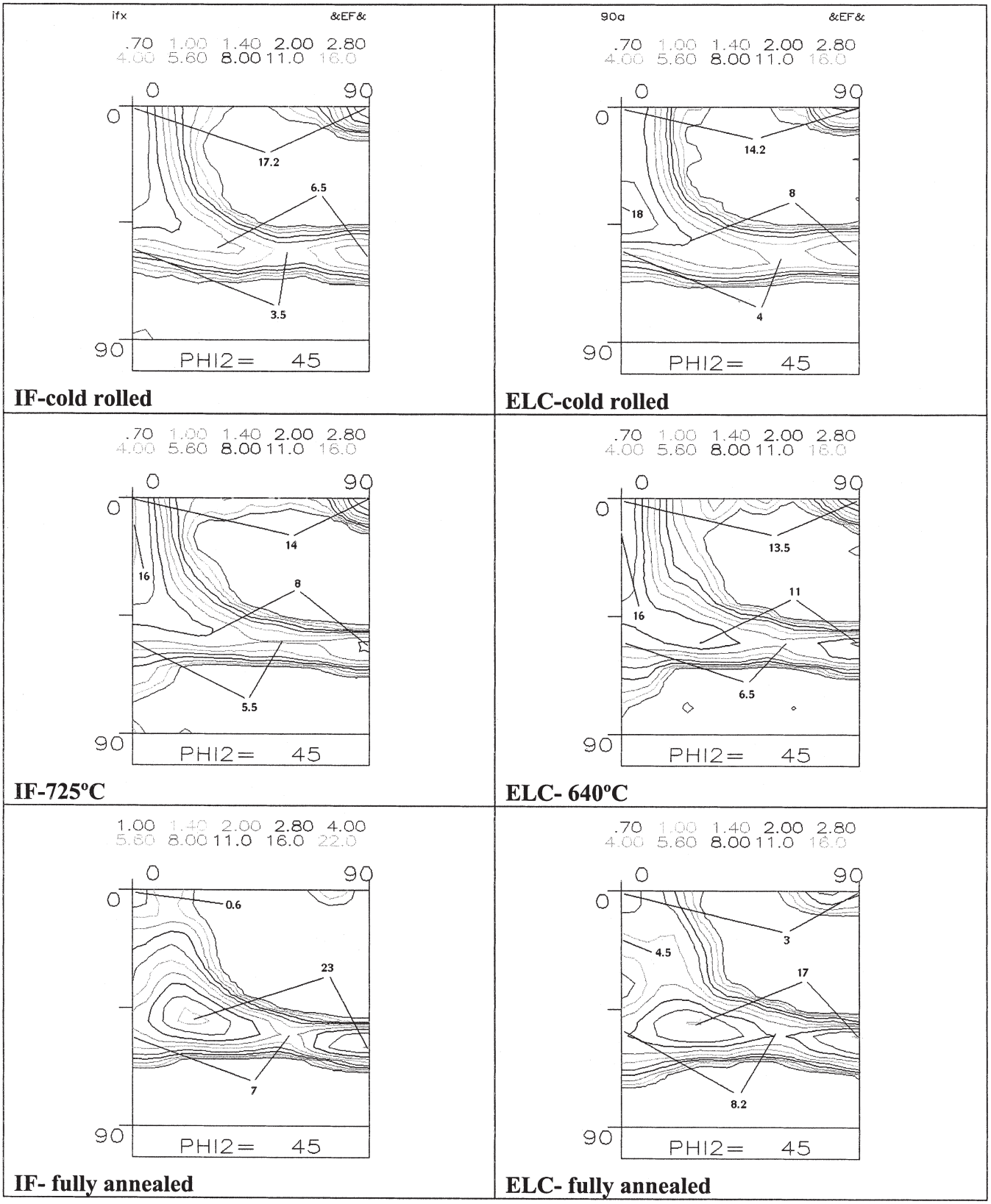

Fig. 4—X-ray ODFs for the cold-rolled and fully-annealed steels.

OIM images have been used to perform quantitative metallography, distinguishing between the different grain classes. Figure 5 shows the effect of the annealing conditions on the proportion of the grains of the different classes. It can be seen that for both steels, the fraction of recrystallized grains with an orientation close to {111} increases with increasing temperature of the annealing cycle. A slight additional increase in the fraction of grains with this orientation is

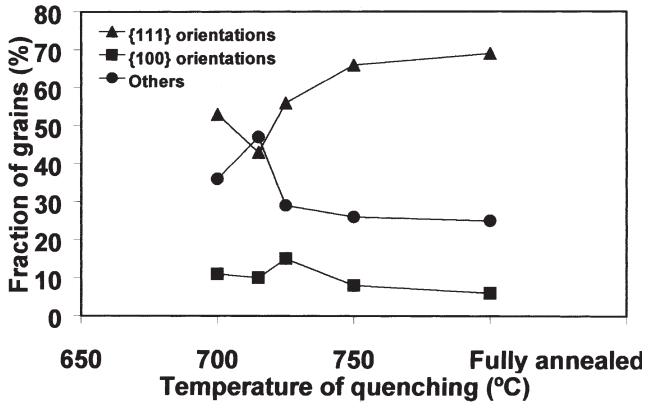

(*a*)

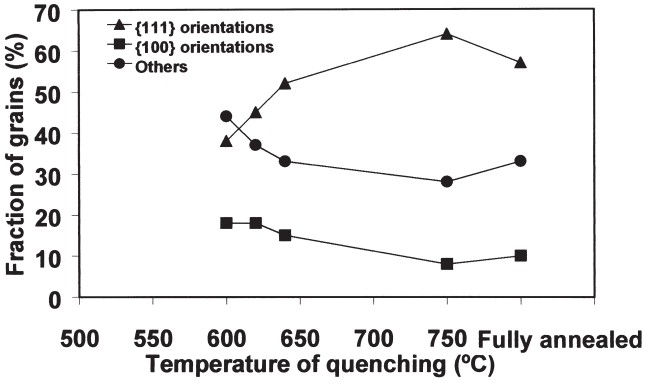

(*b*)

Fig. 5—Evolution of the fraction of the number of recrystallized grains, divided by classes (*a*) IF steel and (*b*) ELC steel.

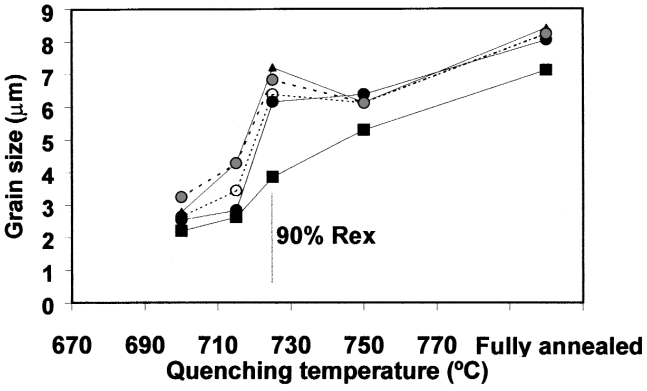

(*a*)

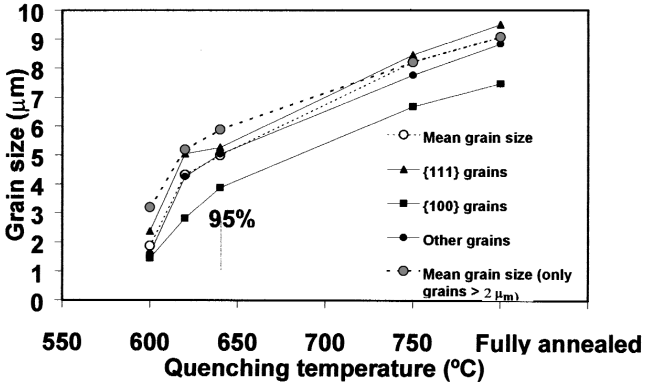

(*b*)

Fig. 6—Grain size evolution in partially and fully recrystallized samples (*a*) IF steel and (*b*) ELC steel.

observed in the fully annealed sample of the IF steel, as compared with the sample quenched from 750 °C. It is interesting to note that in this steel, at the early stages of recrystallization, the {111} grains represent about 50 pct of the grains, the {100} grains represent about 10 pct, and the rest of the grains have other orientations. In the fully annealed condition, the same steel shows about 70 pct of the recrystallized grains being {111}, while only about 5 pct are {100} and the rest have other orientations.

In the ELC steel, the soaking at 750 °C applied in the full annealing cycle seems to produce a slight decrease in the final number of {111} grains. At the first stages of recrystallization, the {111} grains represent, in this steel, about 38 pct of the grains; the {100} grains represent close to 20 pct, and the rest of the grains have other orientations. In the fully annealed condition, the proportion of {111} grains is about 68 pct, while the fraction of grains with other orientations has decreased. At this stage, there are about 10 pct of the grains with a {100} orientation, the rest belonging to other orientations. For both steels, the general trend is that an increase in the number of {111} grains is accompanied by a decrease in both {100} grains and differently oriented grains.

The graphs in Figure 6 show the evolution of the grain size during annealing. The mean grain size is shown, together with the mean sizes of grains with different orientations. It can be seen that, in all the cases, the {111} grains are about 10 pct larger than the mean grain size. This is true for the whole annealing cycle, from the first stages of recrystallization until the fully annealed state. The {100} grains have

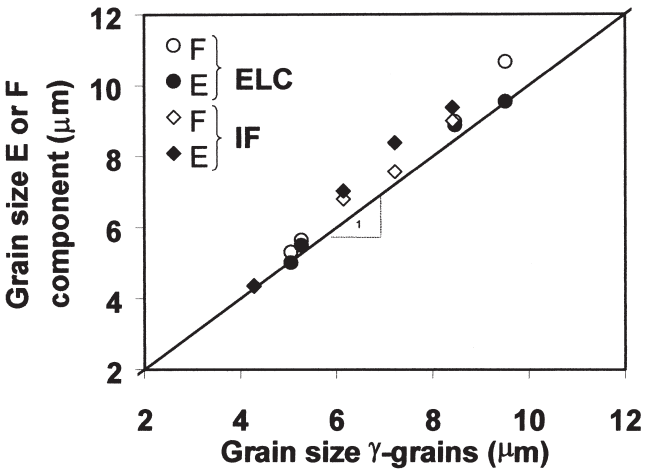

Fig. 7—Mean grain size of F ({111}⟨112⟩) and E ({111}⟨110⟩) components, as a function of the mean grain size of the γ-fiber grains.

sizes significantly lower than the mean size (about 30 pct lower), and the rest of the grains are, in general, about 10 pct lower than the mean. This seems to indicate that the {111} grains, apart from being more numerous, have a size advantage from the first stages of the recrystallization and maintain it throughout the annealing. In Figure 7, the grain sizes of the F and E texture components are compared to those of all grains belonging to the γ-fiber. The line shows the unity slope relation. It can be seen that the size of the

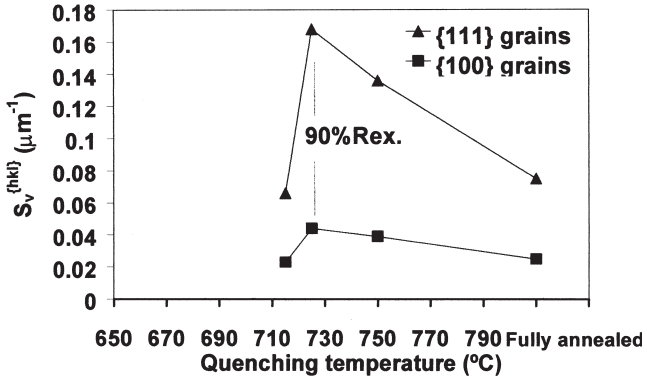

(*a*)

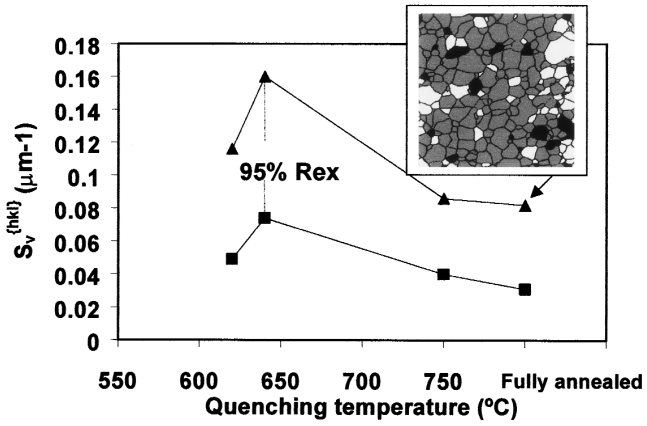

(*b*)

Fig. 8—Interfacial boundary area separating recrystallized {*hkl*} orientation blocks from the rest (recrystallized and nonrecrystallized), as a function of the annealing conditions (*a*) for IF and (*b*) for ELC. The OIM image reveals the orientation of the grains {111}—dark gray, {100}—black, and the remainder of the orientations are in white.

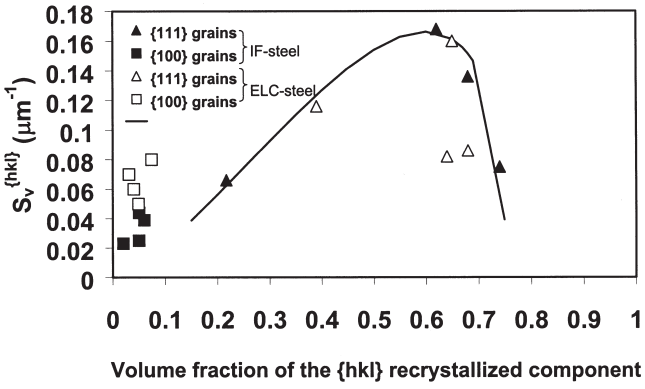

(*a*)

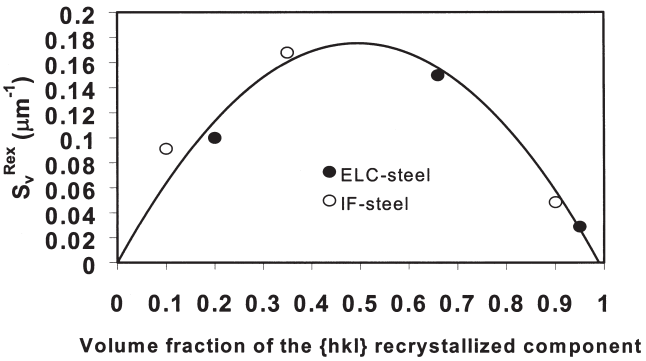

(*b*)

Fig. 9—Interfacial boundary area (*a*) separating recrystallized {*hkl*} orientation blocks from the rest (recrystallized and nonrecrystallized), as a function of the volume fraction occupied by the recrystallized {*hkl*} grains and (*b*) of the recrystallizing front, irrespective of the orientation.

grains of the E and F components starts by being nondistinguishable from that of the rest of the grains belonging to the γ-fiber. However as the temperature increases, E and F component grains become, progressively, larger. No significant differences in behavior are observed between the E and F components in both the ELC and IF steels.

It has been observed that the γ-fiber grains tend to cluster, from the beginning stages of the recrystallization. The clustering of the γ-fiber grains is also evident in the final microstructure obtained with the complete annealing cycle in both steels. An example is shown in the micrograph in Figure 8. The interfacial boundary area ($S_v^{\{111\}}$) separating blocks of recrystallized {111}⟨uvw⟩ grains from the rest of the material (recrystallized or nonrecrystallized) has been determined. The clustering of the {100} grains is much lower, probably caused by the much lower volume fraction they represent. The $S_v^{\{100\}}$ value has also been determined. The results are shown in Figure 8 for both steels. It can be seen that $S_v^{\{hkl\}}$ is significantly higher for the {111} grain clusters and that, for both orientations, it increases during recrystallization and decreases afterward. In Figure 9, the evolution of $S_v^{\{hkl\}}$ has been plotted as a function of the fraction recrystallized. In the same figure, the results corresponding to the area of the migrating front separating recrystallized and deformed regions ($S_v^{\{Rex\}}$), irrespective of their orientation, has also been plotted. It can be seen that the data for both steels follow the same trend, with a maximum value of the migrating-front area for a recrystallized fraction close to 0.5. It is to be mentioned that the maximum values at the peak are very similar for both interfacial areas.

IV. DISCUSSION

By analyzing the evolution of the microstructure during recrystallization, it can be seen that the two steels, in spite of their different compositions which produce modifications on the recrystallization kinetics (Figure 3), exhibit a certain number of points in common.

A. *Nucleation*

From the first stages of the annealing, a network formed by high-angle boundaries (>10 deg) has developed inside the deformed γ-fiber grains (Figure 10). Deformed grains with other orientations have not developed this network. The OIM results obtained in the cold-rolled samples indicate that the quality factor inside the grains with orientations belonging to the γ-fiber is significantly lower than that inside grains with a {001} orientation. This can be related to the heterogeneous distribution of the stored energy during rolling, depending on the orientation of the grains.[5,20] The sequence of decreasing stored energy is, with respect to the main texture components, {111}⟨*uvw*⟩, {211}⟨*uvw*⟩, and {100}⟨011⟩. As a consequence, the nucleation of new grains

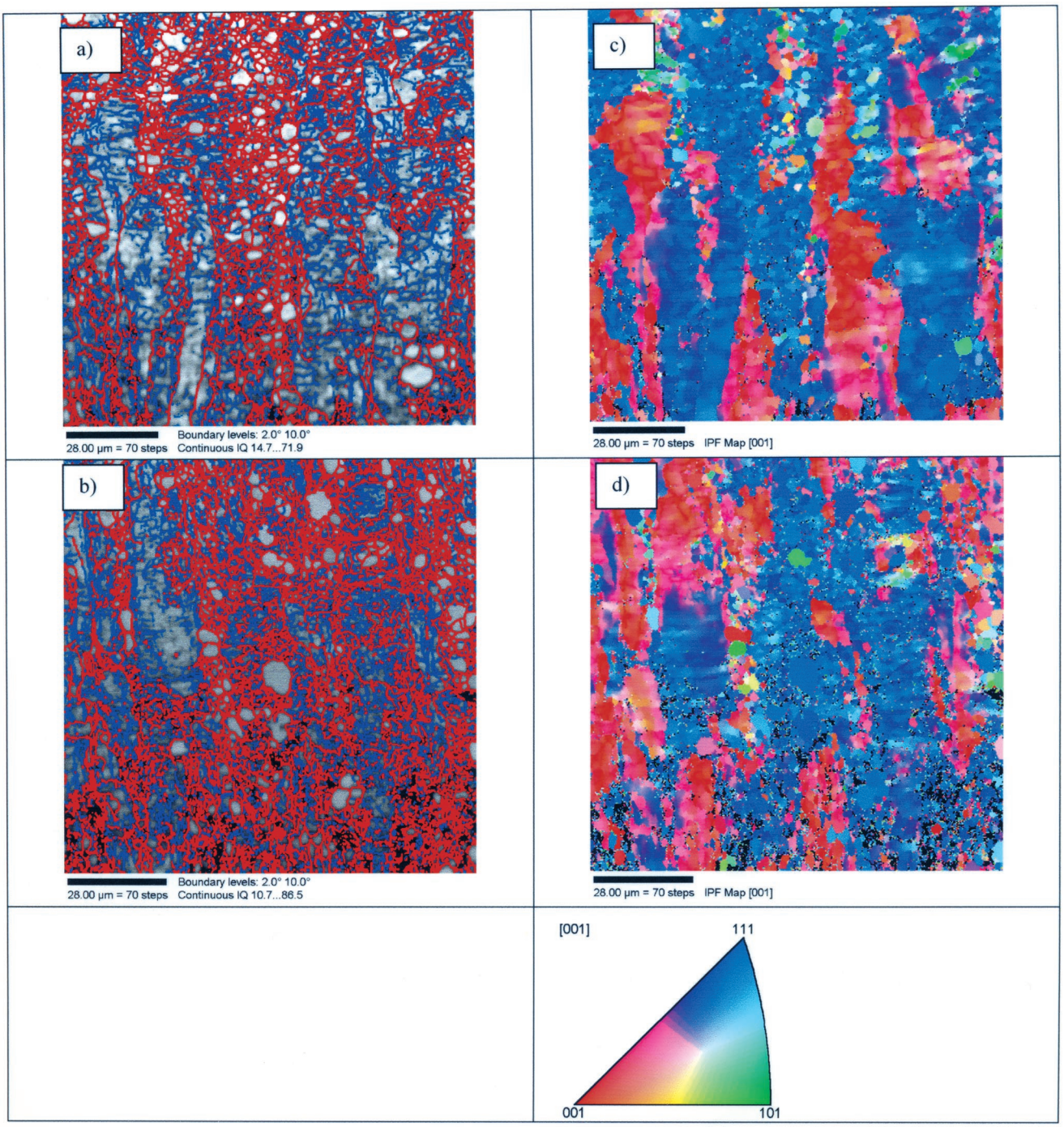

Fig. 10—IQ maps for (*a*) IF and (*b*) ELC steels, where networks of high-angle grain boundaries (>10 deg) in red and low-angle grain boundaries (<10 deg) in blue are observed. The inverse pole figures in (*c*) for IF and (*d*) for ELC show that the high-angle grain boundary networks develop at γ-fiber regions.

is expected to be orientation-sensitive, starting at locations with the highest stored energy.[21] During annealing, the recrystallized grains are observed to nucleate preferentially at locations where the high-boundary network is present and at grain boundaries. This is clearly in agreement with a high-angle boundary network developing by recovery from the deformed microstructure into the {111} grains. The formation of such a network is expected to favor the nucleation of recrystallized grains. The result is a large number of crystallites with small sizes that form clusters, mainly within deformed grains with a {111} orientation (Figures 1 and 2).

When using OIM images, a criterion is required in order to define recrystallized grains. The decision is not straight forward due to a network of crystallites is produced at the first annealing stages, exhibiting the distribution of sizes on the plane of polish shown in Figure 11. The largest of them range within the size interval of 5 to 9μm, while the majority have sizes between 1 and 2 μm. The mean size of the observed crystallites is around 2 μm for both steels. It has been suggested[14] that the nucleation can take place inside γ-fiber grains by abnormal subgrain coarsening. In the same work, it is also indicated that the misorientation between

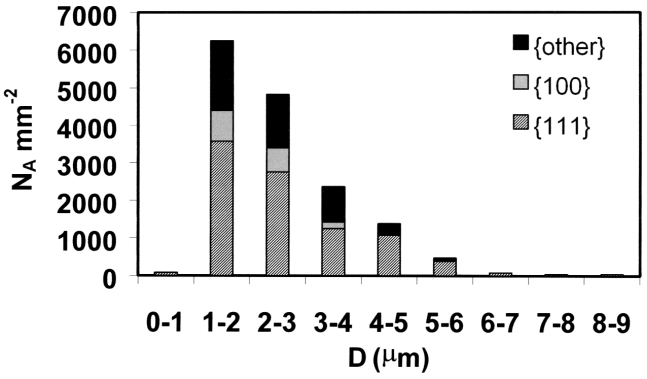

(*a*)

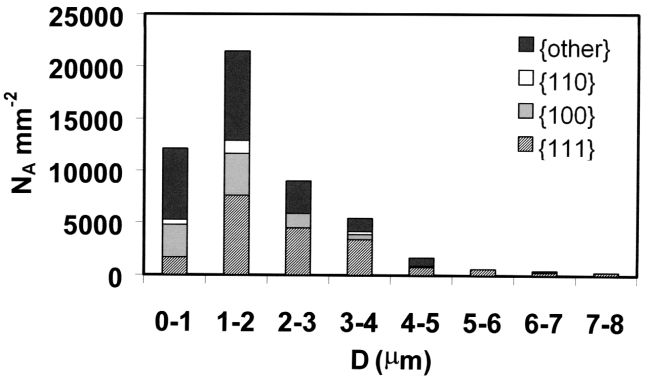

(*b*)

Fig. 11—Number of nuclei/grains per unit area, distinguished by sizes and by orientation in (*a*) IF steel quench from 700 °C and (*b*) ELC steel quench from 600 °C.

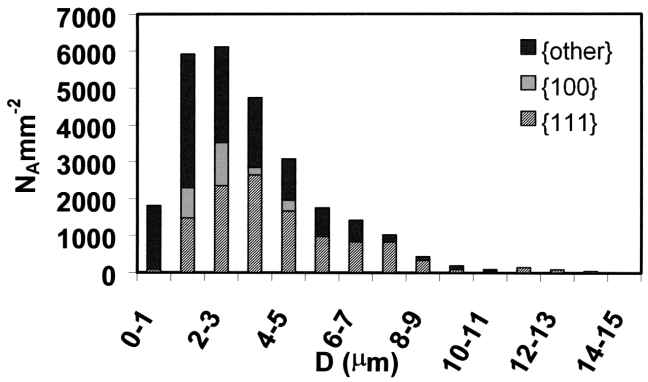

(*a*)

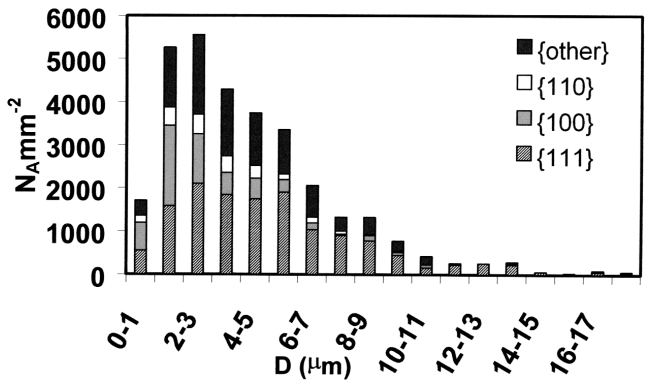

(*b*)

Fig. 12—Number of nuclei/grains per unit area, distinguished by sizes and by orientation in (*a*) IF steel quench from 715 °C and (*b*) ELC steel quench from 620 °C.

subgrains can sometimes exceed 10 deg. This is clearly evident in the present work, in which a large number of crystallites are identified when applying 10 deg as the lower misorientation limit, together with the conditions indicated in the experimental procedure. These crystallites could, in principle, be considered as potential nuclei for recrystallization. For higher temperatures of quenching, the grain-size distribution is shown in Figure 12. It can be seen that the distribution is now much broader than in the previous case. However, small-size crystallites have been produced during recrystallization and/or were formed at the early stages of recrystallization and still remain in the microstructure until the completion of it.

It seems clear that not all the crystallites identified by applying the aforementioned criterion contribute to the final recrystallized microstructure. Probably, only some of them become effective nuclei. A size criterion to distinguish recrystallized grains has been used by some authors. In a work carried out in aluminium,[22] for example, a lower limit of 6 μm^2 has been defined to distinguish recrystallized grains. In other works, sizes of 2 or 3 μm have also been considered as the lower limit for recrystallized grains.[23] The recrystallized fraction in Figure 3 has been determined on the basis of all the crystallites identified according to the 10-deg criterion described in the experimental procedure. If a size criterion considers as recrystallized grains only those crystallites having a size higher than 2 μm, the recrystallized volume fraction is only slightly modified at low fractions, as can be seen in Table II. The mean grain size is also affected, as will be discussed later in Section F.

B. *Kinetics*

The experimental results in Figure 3 show that ELC steel recrystallizes in a lower temperature range than the IF steel. This is the case in general, as reported by other authors,[24] and relates to the retarding effect produced on the recrystallization kinetics by the presence of second-phase particles.[24,25] Additionally, it can be seen that for the case of the ELC steel, the softening data, deduced from hardness measurements, are in good agreement with those obtained from the recrystallized fractions determined by metallography. For the IF steel, larger differences are observed between both sets of data. At low interrupted annealing temperatures, the fraction softened is higher than the recrystallized fraction, which could be an indication of some recovery being active concurrent with recrystallization. This effect is not so evident for the ELC steel, which could be an indication of recovery being less active during the recrystallization of the nonstabilized steel. In a previous work, a good agreement has been found between the recrystallized and the softened fractions in continuously annealed ELC and ultralow-carbon steels.[26,27] During the annealing of iron, the recovery activity has been found to depend on the composition.[27,28] In the case of the IF steel, a ferrite matrix free from the interstitial elements C and N could induce a higher

Table II. Recrystallized Fraction Assuming Different Criteria to Identify Recrystallized Grains by OIM

	X_v					
	ELC			IF		
Temperature of quenching	600	620	640	700	715	725
All the crystallites surrounded by boundaries >10 deg	0.20	0.66	0.95	0.10	0.35	0.90
Only the above crystallites with sizes >2 μm	0.16	0.65	0.94	0.09	0.34	0.90

degree of recovery, as compared with the ELC steel, and this could explain the different behaviors.

The recrystallization curves shown in Figure 3 have been deduced from a model developed elsewhere.[29] This model uses the Scheil theory[30] to determine the recrystallization kinetics under the nonisothermal heating conditions used in continuous annealing cycles. The model was deduced for ELC and ultralow carbon steels and takes into account the free nitrogen and carbon contents and the hot-band grain size and applies, satisfactorily, to the present ELC steel. In the case of the IF steel, the model cannot be directly applied, because the recrystallization has been delayed by the effect of precipitates. The pre-exponential factor in the Avrami equation has been adapted to fit the experimental data, but the same activation energy of 280 kJ/mol[31] and exponent of n = 1 for the ELC steel have been used (continuous line in the figure). It can be seen that a reasonable agreement is obtained mainly for the softening data. The recrystallized fractions fit better to the predictions of the model (hatched line) if an activation energy of 500 kJ/mol, as reported to describe the recrystallization kinetics of an IF steel,[24] is used, together with the exponent $n = 1$.

C. *Texture*

The ODFs in Figure 4 show the usual transition from cold-rolling textures formed basically by intensity along the rolling direction//$\langle 110 \rangle$ α-fiber, ND//$\langle 111 \rangle$ γ-fiber, and some intensity of cube components,[32] to the recrystallization texture. As can be seen in the figures, during the annealing cycle, the cube component progressively disappears, and the α-fiber loses part of its intensity, which concentrates around the γ-fiber. It has to be mentioned that the main changes, with respect to the γ-fiber development in the ODFs, take place close to the completion of the recrystallization. This is true for both steels and has also been reported by other authors.[33] In the ODFs obtained from the fully annealed samples, the γ-fiber shows two maxima close to the positions of the F:$\{111\}\langle 112 \rangle$ and E:$\{111\}\langle 110 \rangle$ components. However, due to the curvature of this fiber, these maxima displace in both cases toward $\{554\}\langle 225 \rangle$. The curvature of the γ-fiber is a key characteristic in deep-drawable steels[34] and has been explained in terms of the allowed rotations, relating the recrystallization texture to that produced by cold rolling and to the selective growth of certain orientations.[35,36]

A difference between both steels is the presence of some grains with the {110} orientation at the early stages of the recrystallization in the ELC steel. These grains are no longer present at the end of the recrystallization and are not observed in the IF steel. In spite of the fact that this orientation has been observed by EBSD, it does not appear in the global texture X-ray ODFs, probably due to its relatively low volume fraction. It can also be seen that the relation between γ-fiber grains and other oriented ones is higher in the IF steel than in the ELC steel.

D. *Microtexture and Grain Sizes*

From Figure 5, it can be deduced that the fraction of recrystallized grains with {111} orientations and with other orientations (different from {111} and {100}) are comparable during the first stages of the annealing, but diverge afterward. The fraction of {111} grains increases, at the expense of the number of grains with other orientations. The same trend is observed for both steels, even if the fraction of γ-fiber grains in the IF steel is higher than in the ELC steel. Close to the completion of recrystallization, the fraction of the γ-fiber grains is close to 60 and 50 pct, respectively. The mean grain size of the γ-fiber grains is only about 10 pct higher than the mean, (Figure 6); accordingly, the fraction of grains can be compared to the volume fractions of different components deduced by other authors in ULC[37] and Ti-bearing IF[38,39] steels. A good agreement is obtained. The cube grains have mean grain sizes about 20 to 25 pct lower than the mean. In the present ELC and IF steels, their number fraction is about 15 pct, while the volume fraction they represent is around 10 pct at the end of the recrystallization, this last value being approximately the same value as that previously reported.[37,38]

In Figure 6, the evolution of the mean grain size of all the crystallites identified according to the 10-deg criterion is shown, for different orientations. The mean grain size for grains with sizes higher than 2 μm has also been plotted for comparison. It can be seen that some significant differences are observed between both. These are more important at low recrystallized fractions, but remain until the completion of recrystallization. The γ-fiber grains have a size and number advantage as compared to the cube grains, which is in agreement with previous results.[4,11] From the point of view of optimum texture development, the relation between the F and E components is important. Figure 7 shows that a size advantage is not observed for the E or F grains with respect to the mean size of γ-fiber grains. These results are in agreement with the results by other authors,[38] who found that the F and E components grow at almost the same rate. However, some advantage in the number and volume fraction of the F components has been observed, in agreement with other published results.[23]

Coming back to the results in Figure 6, it can be observed that the variation of the size with the conditions of the cycle follows the same trend, independent of the steel and the considered orientation of the grains. Two ranges can be distinguished. During recrystallization, the evolution of the grain size with the temperature of the cycle is much more pronounced than afterward. This can be explained as follows.

Table III. Different Apparent Rates, as Defined in the Text

	(μ/s)	IF Steel	ELC Steel
Recrystallization	$F'_{\{111\}}$	1	0.43
	$F'_{\{100\}}$	0.40	0.4
Grain growth	$F'_{\{111\}}$	—	0.16
	$F'_{\{100\}}$	0.3	0.13
Recrystallization ($X_v \approx 0.5$)	$G^*_{\{111\}}$	1.1	0.6
	$G^*_{\{100\}}$	0.36	0.2
Grain growth ($X_v \approx 1$)	$G^*_{\{111\}}$	0.08	0.07
	$G^*_{\{100\}}$	0.03	—
Recrystallization ($X_v \approx 0.5$)	G^*_{Rex}	1.1	0.64

During recrystallization, two types of mechanisms are expected to have an effect on the grain-size evolution. The first is the grain coarsening produced by the movement of the recrystallizing front and driven by the cold-work stored energy. Additionally, some normal grain growth among impinged recrystallized grains can happen behind the recrystallization front driven by the curvature of the grain boundaries. The magnitude of both contributions to the recrystallized grain size is difficult to separate. However, after recrystallization is complete, only the second mechanism can be operative, as the stored energy of deformation has vanished. The driving force for grain-boundary migration induced by cold-work stored energy is significantly higher than the driving force for the normal grain growth. Accordingly, it seems reasonable that the grain-size coarsening rate be higher during recrystallization than after it, and this explains the change in slope observed experimentally in the graphs of Figure 6 when recrystallization goes to completion. These slopes are related to the grain coarsening rate, irrespective of the mechanism driving it (recrystallization or normal grain growth).

According to the present results, it can be supposed that the effect of the normal grain growth behind the recrystallization front is responsible for about 20 pct of the total grain-coarsening rate. In the case of the {100} grains, the apparent rate during grain growth has been found to be zero, or even slightly negative. This last finding is an indication of the α-fiber grains being consumed at this stage.

E. *Apparent Growth Rates*

In the present work, nonisothermal conditions have been applied during annealing; consequently, the previously mentioned rate cannot be deduced. Under nonisothermal conditions, the grain size can be expressed as a function of time and temperature in the form $f(T(t),t) = F(t)$ or as $g(T, t(T)) = G(T)$, and

$$\left.\frac{\partial F}{\partial t}\right|_T = F'(t) - \left.\frac{\partial F}{\partial T}\right|_t \frac{dT}{dt} \qquad [2]$$

The derivative F' can be calculated from the plot of the volume fraction as a function of time, or, alternatively, as

$$F'(t) = G'(T)\frac{dT}{dt} \qquad [3]$$

The first term in Eq. [2] cannot be deduced from the present set of results, obtained under continuous heating conditions. However, by using $F'(t)$, an apparent coarsening rate can be deduced, including the effect of time and temperature. The obtained results are shown in Table III. To be noted are the higher apparent coarsening rates in IF steel, as compared with the ELC steel, probably due to the different range of temperatures. It is clear that the grain coarsening is much lower after recrystallization than during it.

In Figure 9(a), the interfacial boundary area separating recrystallized {hkl}-oriented blocks from the rest (recrystallized and nonrecrystallized), as a function of the volume fraction occupied by the recrystallized {hkl} grains, is represented. It can be seen that the shape of the obtained curve is similar to that encountered in general for recrystallization, even if what is being plotted now is different. It can be seen that initially, the interfacial area limiting recrystallized regions with a {111} orientation increases with the volume fraction of these same regions, until a fraction of about 0.6. This fraction corresponds approximately to that of the γ-fiber grains at the end of the recrystallization. After recrystallization is complete, there is a dramatic drop of the interfacial area and, by extrapolation, it seems that a volume fraction of {111}-oriented regions higher than about 75 pct cannot be reached. The sudden drop in such an area is probably due to a hard clustering of {111} grains. The line in Figure 9(a) has been fitted to the experimental data obtained from both steels, by using the type of semiempirical equation proposed by Rath,[40] according to the following expression:

$$S_v^{\{111\}} = 0.66(X_v^{\{111\}})^{1.4}(0.75 - X_v^{\{111\}})^{0.35} \qquad [4]$$

This formulation cannot be applied to the {001} grains whose volume fraction is much lower.

In the case of the area between recrystallized and deformed regions, shown in Figure 9(b) as a function of the fraction recrystallized, the following expression has been found to fit to the experimental data for both steels:

$$S_v^{\text{Rex}} = 0.70\, X_v\,(1 - X_v) \qquad [5]$$

This last equation gives a symmetrical function with a peak at a recrystallized fraction of 0.5. The S_v^{Rex} term represents the unimpinged surface area of the nuclei/grains, and a symmetrical function of it with the fraction recrystallized is associated with a random type of nucleation. However, the shape of this curve cannot be considered to be conclusive by itself.[41]

Cahn and Hagel[42] defined the interface-averaged grain-boundary migration (G) according to the following expression:

$$G = \frac{1}{S_v}\frac{dX_v}{dt} \qquad [6]$$

Hutchinson and Ryde[43] applied this equation after isothermal annealing tests, to compute the mean interface grain-boundary migration rate at constant temperature for different texture components at recrystallized volume fractions between 20 and 45 pct. The data they obtained showed that {111} orientations have a growth advantage, as a result of a rate (0.063 μm/s) about 20 pct higher than that of the non-{111} grains. In another work,[44] it has been found that there is no difference in growth rate between different {111}$\langle uvw \rangle$ texture components and that the rate decreases during recrystallization from about 0.01 to 0.001 μm/s. Other authors determine that the mean interface grain-boundary migration rate of the different main components of the γ-fiber are not significantly different from those of the {001} or {112} grains. The rates they found range between 0.0023 and 0.029 μm/s

and seem to remain approximately constant during recrystallization.

Equation [6] cannot be applied directly, because the tests have been carried out under nonisothermal conditions. Like in the case of the grain-size coarsening, an apparent migration rate can be considered, applying Eq. [3]. In this way, the apparent unimpinged interface grain-boundary migration rate ($G^*_{\{hkl\}}$) of recrystallized regions with a given {hkl} orientation, for a constant heating rate of 6 °C/s, has been calculated. The average is done over an interface separating two recrystallized regions with different orientations and for an interface between recrystallized and nonrecrystallized areas. Consequently, the apparent mean migration rate gives an indication of the movement of the interface-separating clusters of {*hkl*} grains from their surroundings, irrespective of whether these last are recrystallized.

Applying this to the experimental data, the results in Table III are obtained. It can be seen that the growth rates are again higher in the IF steel than in the ELC steel. An additional difference is observed between both steels. In the case of the ELC steel, the migration rate of the {111} front is similar to that of the {100} front, even if, in agreement with the results in Figure 5, the number of {100} grains tends to decrease during annealing. For the IF steel, the {111} front moves significantly faster than the interface-delimiting {100} grains.

Two ranges of migration rates have been deduced; the first of them corresponds to the incomplete recrystallization range and the second to the grain-growth range after recrystallization is complete. It is important to note that the apparent migration rate of the {111} front slows down approximately by 90 pct once the recrystallization is complete. This is consequent with the lower driving force for migration in normal grain growth, as compared with that driving the motion of the recrystallization front.

The same type of formulation can be applied to define an apparent migration rate for the recrystallization front. This gives the mean apparent rate for the recrystallization front (G^*_{Rex}) at X_v around 0.5, shown in Table III. It can be seen that these apparent rates are seemingly similar to those obtained for ($G^*_{\{111\}}$), which seems reasonable, taking into account that this last result has a contribution coming from migration behind the recrystallization front.

F. *General Considerations*

In Figure 13, the evolution of the mean grain size (D_x), measured from the OIM images, has been plotted as a function of the recrystallized volume fraction. The lines correspond to the following equation:

$$D_x = D_{\mathrm{Rex}} X_v^{1/3} \qquad [7]$$

Where D_{Rex} is the mean recrystallized grain size at the end of recrystallization. This equation is only applicable if the recrystallization progresses under the conditions of site saturation, uniform growth, and all the formed grains remaining until the end of recrystallization. This equation does not apply when all the nuclei/grains defined according to the 10-deg criterion are considered to contribute to the mean grain size. However, when a restriction to this criterion is applied, considering, for example, only grains larger than 2 μm in diameter, a good agreement is reached between the predictions of Eq. [7] and the experimental results, as can be seen in Figure 13. The effect of taking a different criterion to identify the recrystallized grains has a larger effect on the ELC than on the IF steel, which is a point that would need to be investigated more in depth.

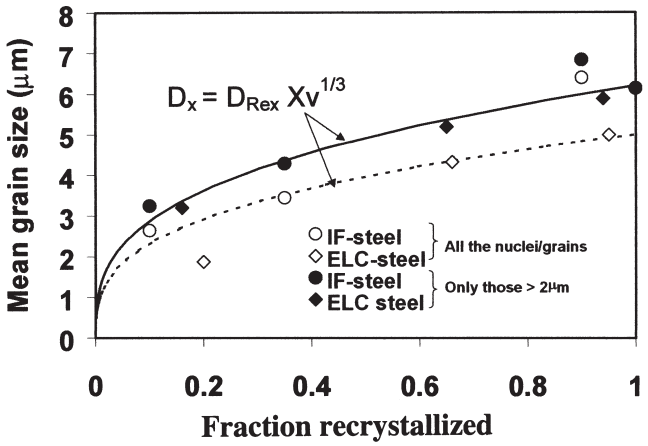

Fig. 13—Mean nuclei/grain size as a function of the recrystallized fraction.

When applying the 10-deg criterion, the crystallites being observed can be interpreted as being potential nuclei produced, probably, by recovery mainly into {111} regions. However, these crystallites are much higher in number than those being really effective concerning the evolution of the recrystallization. One of the reasons for it can be the hard impingement due to the clustered nature of their formation (Figures 1 and 2). From all of them, only those having boundaries with a high mobility are expected to become effective nuclei.[45,46] The final result, in terms of kinetics, seems to be in agreement with site saturation. Very small crystallites are present all along the recrystallization process, but the experimental results do not suggest that they are the result of some nucleation being concurrent with recrystallization. The nucleation is clearly not homogeneous, but, taking into account the nuclei selection that seems to be operative during the first stages of the recrystallization, the final behavior is very similar to what is expected in the case of homogeneous formation of new grains. This is possible due to the fact that only very few of the potential nuclei become effective and significant from the point of view of recrystallization. The rest of the crystallites seem to remain in the microstructure until the advance of the recrystallization front finally consumes them.

V. CONCLUSIONS

1. During the annealing of the cold-rolled IF and ELC steels, the formation of a network of high-angle boundaries seems to be orientation-sensitive, starting at the locations with the highest stored energy, which concentrate around {111}⟨uvw⟩ γ-fiber orientations. This network leads to the formation of clustered crystallites surrounded by boundaries >10 deg. These crystallites can be considered as potential nuclei, even if only some of them become effective nuclei (probably, those surrounded by the highest-mobility boundaries).
2. The main changes, with respect to the γ-fiber development in the ODFs, take place at the latest stages of recrystallization. For the fully annealed condition, the γ-fiber

shows a characteristic curvature that has been associated with good drawing properties.

3. From analysis carried out by OIM, a close correlation appears between the increasing fraction of {111}-type grains and the decreasing of fraction of {100}-type and differently oriented grains from the early stages of recrystallization to the fully anneal condition, both for the IF and the ULC steels. The growth advantage of {111}-type grains to differently oriented grains is evident from the early stages of recrystallization, although it is slightly higher for the IF steel. The increased number of grains with this particular orientation could be associated with a "frequency-advantage" mechanism.
4. The {111} grains exhibit a 10 pct larger than average grain size. This "size advantage" operates from the first stages of the recrystallization to the fully annealed condition, independently of the steel. A hard impingement between {111} grains is effective when all the deformed microstructure is consumed.
5. Grain coarsening is faster during recrystallization than during the grain-growth stage, due to a significantly higher driving force for the recrystallization mechanism. The apparent migrating rate is reduced by 90 pct after the completion of recrystallization, which is an indication of the grain-growth contribution behind the recrystallization front being negligible.
6. Due to an intense selection, only some of the potential nuclei become active and, from a macroscopic point of view, this seems to behave according to homogeneous nucleation, site saturation, and almost normal grain growth.

REFERENCES

1. R.C. Hudd: *Processing, Cold Working and Annealing*, Materials Science and Technology, F.B. Pickering, eds., VHC, Germany, 1991, vol. 7, pp. 219-84.
2. M. Abe: *Processing, Cold Working and Annealing*, Materials Science and Technology, F.B. Pickering, ed., VHC, Germany, 1991, pp. 285-333.
3. W.B. Hutchinson: *Int. Mater. Rev.*, 1984, vol. 29(1), pp. 25-42.
4. R.K. Ray, J.J. Jonas, and R.E. Hook: *Int. Mater. Rev.*, 1994, vol. 39 pp. 129-72.
5. I.L. Dillamore, C.J.E. Smith, and T.W. Watson: *Met. Sci. J.*, 1967, vol. 1, pp. 49-54.
6. B.F. Decker and D. Harker: *J. Appl. Phys.*, 1951, vol. 22, pp. 900-04.
7. B. Hutchinson and L. Ryde: in *Thermomechanical Processing in Theory, Modelling and Practice*, B. Hutchinson, M. Anderson, G. Engberg, B. Karlsson, and D. Siwecki, eds., Stockholm, 1996, pp. 145-61.
8. K. Lücke: *Can. Metall. Q.*, 1974, vol. 13, pp. 261-74.
9. G. Ibe and K. Lücke: *Arch. Eisehüttenwes*, 1968, vol. 39, pp. 693-703.
10. I. Samajdar, B. Verlinden, P. Van Houtte, and D. Vanderschueren: *Mater. Sci. Eng.*, 1997, vol. A238, pp. 343-50.
11. B. Verlinden, I. Samajdar, and P. Van Houtte: *4th Int. Conf. on Recrystallisation and Related Phenomena*, Eds. T. Sakai and H.G. Susuki, eds., The Japan Institute of Metals, Tsukuba, Japan, 1999, vol. 3, pp. 373-78.
12. L. Kestens and J.J. Jonas: *Met. Mater.*, 1999, vol. 5, pp. 419-27.
13. L. Kestens, K. Verbeken, and J.J. Jonas: *Proc. 1st Joint Int. Conf. on Recrystallization and Grain Growth*, G. Gottstein and D.A. Molodov, eds., Springer-Verlag, New York, NY, 2001, vol. 2, pp. 695-706.
14. H. Réglé: *Proceedings of the First Joint International Conference on Recrystallization and Grain Growth*, G. Gottstein and D.A. Molodov, eds., Springer-Verlag, New York, New York, 2001, vol. 2, pp. 707-17.
15. D. Juul Jensen: *Acta Metall. Mater.*, 1995, vol. 43(11), pp. 4117-25.
16. M.T. Lyttle and D. Juul Jensen: *4th Int. Conf. in Recrystallization and Related Phenomena*, T. Sakai and H.G. Suzuki, eds., The Japan Institute of Metals, Tsukuba, Japan, 1999, pp. 185-90.
17. D. Juul Jensen: *Proc. 2nd Int. Conf. on Grain Growth in Polycrystalline Materials, Part 2*, H. Yoshinaga, T. Watanabe, and N. Takahashi, eds., Transtec Publications, Kitakyushu, Japan; *Mater. Sci. Forum*, 1995, vols. 204–206, pp. 713-22.
18. F.J. Humprheys and M. Hatherly: *Recrystallization and Related Annealing Phenomena*, Elsevier Science Ltd., Oxford, United Kingdom, 1996, pp. 173-220.
19. P. Van Houtte: *Manual of MTM-FHM*, MTM-KU, Leuven, Belgium, 1995.
20. H. Takechi, H. Kato, and S. Nagashima: *Trans. TMS-AIME*, 1968, vol. 242, p. 56.
21. W.B. Hutchinson: *Met. Sci.*, 1974, vol. 8, pp. 185-96.
22. D. Juul Jensen: *Proc. 4th Int. Conf. on Recrystallization and Related Phenomena*, T. Sakai and H.G. Suzuki, eds., The Japan Institute of Metals, Tsukuba, Japan, 1999, vol. 13, pp. 3-14.
23. I. Samajdar, B. Verlinden, and P. Van Houtte: *Acta Mater.* 1998, vol. 46, pp. 2751-63.
24. K. Mukunthan and E.B. Hawbolt: *Metall. Mater. Trans. A*, 1996, vol. 27A, pp. 3410-23.
25. D.O. Wilshynsky, G. Krauss, and D.K. Matclock: *Proc. Int. Symp. on Interstitial Free Steel Sheet: Processing, Fabrication and Properties*, L.E. Collins and D.L. Baragar, eds., CANMET, Ontario, Canada, 1991, pp. 69-79.
26. M.M. Petite: PhD. Thesis, University of Navarra, San Sebastian, 1999.
27. W.C. Leslie, F.J. Plecity, and J.T. Michalack: *Trans. TMS-AIME*, 1961, vol. 221, pp. 691-700.
28. G. Venturello, C. Antonione, and F. Bonaccorso: *Trans. TMS-AIME*, 1963, vol. 227, pp. 1433-39.
29. I. Guttiérrez, M.M. Petite, J.I. Larburu, J. Zaitegui, W.B. Hutchinson, D. Artymowicz, P.J. Evans, G.J. Spurr, H.K.D.H. Badhesia, and N. Chester: *Modelling of Microstructural Development During Continuous Annealing Process*, Technical Steel Research, EUR 19877 EN, Office for Official Publications of the European Communities, Luxembourg, Luxembourg, 2001.
30. E. Sheil: *Arch. Eisenhuttenwes*, 1935, vol. 12, pp. 565-67.
31. K. Magee, K. Mukunthan, and E.B. Hawbolt: *Proc. Int. Conf. on Recrystallization in Metallic Materials*, T. Chandra, ed., TMS, Warrendale, PA, 1990, pp. 393-98.
32. T. Urabe and J.J. Jonas: *Iron Steel Inst. Jpn. Int.*, 1994, vol. 34, pp. 435-42.
33. J.J. Jonas and L. Kestens: *Proc. 1st Joint Int. Conf. on Recrystallization and Grain Growth, Vol. 2*, G. Gottstein and D.A. Molodov, eds., Springer-Verlag, New York, NY, 2001, pp. 49-60.
34. L. Kestens and J.J. Jonas: *Met. Mater.*, 1999, vol. 5, pp. 419-27.
35. P. Gangli, L. Kestens, and J.J. Jonas: *Metall. Mater. Trans. A*, 1996, vol. 27A, pp. 1-9.
36. J.J. Jonas and L. Kestens: *Proc. 2nd Int. Conf. on Grain Growth in Polycrystalline Materials*, H. Yoshinaga, T. Watanabe, and N. Takahashi, eds., Transtec Publications, Kitakyushu, Switzerland; *Materials Science Forum*, 1995, vols. 204–206, pp. 155-68.
37. B. Verlinden, I. Samajdar, P. Van Houtte, and L. Kestens: *Proc. Microalloying in Steels*, J.M. Rodriguez-Ibabe, I. Guttiérez, and B. López, Trans Tech Publications, Aedermannsdorf, Switzerland; *Mater. Sci. Forum*, 1998, vols. 284–286, pp. 527-34.
38. I. Samajdar, B. Verlinden, and P. Van Houtte: *Acta Mater.*, 1998, vol. 46, pp. 2751-63.
39. H. Magnusson, D. Juul Jensen, and B. Hutchinson: *Scripta Mater.*, 2001, vol. 44, pp. 435-41.
40. B.B. Rath: in *Solid-Solid Phase Transformations*, H.I. Aaronson, D.E. Laughlin, R.F. Sekerka, and C.M. Wayman, eds., TMS-AIME, Warrendale, PA, 1982, pp. 1097-1103.
41. D. Juul Jensen: *Proc. 1st Joint Int. Conf. on Recrystallization and Grain Growth, Vol. 1*. G. Gottstein and D.A. Molodov, eds., Springer-Verlag, New York, NY, 2001, pp. 73-86.
42. J.W. Cahn and W.C. Hagel: *Acta Metall.*, 1963, vol. 11, pp. 561-74.
43. B. Hutchinson and L. Ryde: *Proc. 16th Risø Int. Symp. on Material Science: Microstructural and Crystallographic Aspects of Recrystallization*, Roskilde, Denmark, 1995, N. Hansen, D. Juul Jensen, Y.L. Liu, and B. Ralph, eds., Roskilde, Denmark, pp. 105-17.
44. H. Magnusson, D. Juul Jensen, and B. Hutchinson: *Scripta Mater.*, 2001, vol. 44, pp. 435-41.
45. D. Juul Jensen: *Proc. 16th Risø Int. Symp. on Material Science*, Roskilde, Denmark, N. Hansen, D. Juul Jensen, Y.L. Liu, and B. Ralph, eds., Roskilde, Denmark, 1995, pp. 119-37.
46. D. Juul Jensen: *Proc. 3rd Int. Conf. on Recrystallization and Related Phenomena*. T. McNelley, ed., Monterey Institute of Advanced Studies, Monterey, CA, 1997, pp. 15-30.